Cubosome-Induced Topological Transformations in Giant Vesicles

Zexi Xu[1,2], Michael Rappolt[1], Arwen I.I. Tyler[1*], Paul A. Beales[2*]

[1] School of Food Science and Nutrition, University of Leeds, Leeds, LS2 9JT, United Kingdom

[2] School of Chemistry and Astbury Centre for Structural Molecular Biology, University of Leeds, Leeds, LS2 9JT, United Kingdom

*Corresponding authors

Arwen I.I. Tyler; e-mail: A.I.I.Tyler@leeds.ac.uk

Paul A. Beales; e-mail: P.A.Beales@leeds.ac.uk

Abstract

Lipid nanoparticles have important applications as biomedical delivery platforms and broader engineering biology applications in artificial cell technologies. These emerging technologies often require changes in the shape and topology of biological or biomimetic membranes. Here we show that topologically-active lyotropic liquid crystal nanoparticles (LCNPs) can trigger such transformations in the membranes of giant unilamellar vesicles (GUVs). Monoolein (MO) LCNPs with an internal cubic nanostructure of space group Im3m incorporate into 1,2-dioleoyl-sn-glycero-3-phosphocholine (DOPC) GUVs creating excess membrane area with stored curvature stress. Using real-time fluorescence confocal microscopy, we observe and characterise various life-like dynamic events in these GUVs, including growth, division, tubulation, membrane budding and fusion. Our results shed new light on the interactions of LCNPs with bilayer lipid membranes, providing insights relevant to how these nanoparticles might interact with cellular membranes during drug delivery and highlighting their potential as minimal triggers of topological transitions in artificial cells.

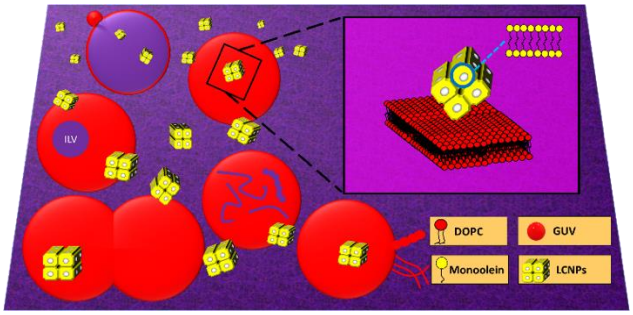

Keywords: Artificial cells, nanomedicine, membrane remodelling, lyotropic liquid crystal nanoparticles, cubosomes, lipids, vesicles

Introduction

Lipid-based nanostructures are fundamental structures in nature, providing the structural basis of organelles that support localised intracellular and extracellular biochemical functions within living organisms.[1, 2, 3] These structures have inspired a range of biotechnological developments, including nanoparticulate formulations for enhanced therapeutic delivery.[4, 5, 6] Lipids can self-assemble into a broad array of different nanostructures dependent on their molecular shape, which gives rise to a preferred interfacial curvature in their assembled supramolecular state.[7, 8] This rich lipid polymorphism gives rise to a broad range of tuneability in the properties of lipid-based formulations.[4, 7] Curved 3D membrane networks known as cubosomes have been of particular recent interest; their high interfacial surface area gives a high capacity for drug loading and interfacial chemical processes within an individual nanoparticle.[9] Therefore cubosomes are of broad interest within nanomedicine and bottom-up approaches to synthetic biology through the design of artificial cells. The internal structure of cubosomes consists of highly curved lipid bilayers being draped around a periodic minimal surface creating two distinct continuous 3D-networks of water channels (**Fig. 1a,b**).

Real cells and many artificial cells are bound by a lipid bilayer membrane as their intrinsic structural matrix. Therefore understanding the interactions between lipid cubic phases and lamellar lipid bilayer structures is fundamental to improving our understanding of drug delivery mechanisms and potential bio-engineering applications within artificial cells. Essential to the functionality of biological membranes is their ability to undergo dynamic shape and topology transformations involved in critical cell activities such as growth, division and trafficking.[10, 11] In nature, a range of protein complexes are involved in the regulation of these membrane remodelling events by a range of active and passive interaction mechanisms that scaffold, bend and cut the membrane as required, including the ESCRTs (endosomal sorting complex required for transport), SNAREs (soluble N-ethylmaleimide-sensitive fusion protein attachment protein receptors), caveolin, dynamin and cytoskeletal filaments.[12, 13, 14, 15] However, the fluidity and flexibility of these interfacial membrane structures are key to these

processes and the energy barriers to topological transitions are regulated by lipid composition and the intrinsic curvature stress stored within these membranes, where the shape of lipid molecules influence the lateral stress profile across a bilayer membrane.[16, 17, 18] Therefore seeding lipid bilayer membranes with curved lipid structures such as cubosomes has the potential to enhance their topological activity.

The interaction of lyotropic liquid crystal nanoparticles (LCNPs) such as cubosomes with surfaces has been extensively studied.[19, 20, 21] Of particular interest are their interactions with lipid membrane interfaces, where insight has previously been provided using solid-supported lipid bilayers.[22, 23] These studies suggest a strong and rapid attraction between LCNPs and supported DOPC lipid bilayers on silica.[23] Once sufficient LCNPs incorporate into the supported bilayer, this leads to destabilisation of its structure and a net release of material from the bilayer; QCM-D revealed the lipid surface becomes viscoelastic with a large change in dissipation following addition of LCNPs.[23] Moreover, a significant lipid exchange between the hydrogenated monoolein (MO) LCNPs and the deuterated DOPC lipid bilayer was confirmed by neutron reflectivity, revealing bidirectional transfer of MO to the supported bilayer and DOPC to the LCNPs.[23] By contrast, the incorporation of LCNPs into supported bilayers was hindered in more organised lipid bilayers in the gel phase, where dipalmitoylphosphatidylcholine (DPPC) lipids densely pack in an orthorhombic fashion.[24] Complementary small angle X-ray scattering (SAXS) results confirmed that LCNPs have a strong interaction with DOPC unilamellar and multilamellar vesicles: large changes in the unit cell dimensions of the LCNPs were observed, eventually resulting in a transition from a cubic to lamellar phase structure once DOPC and MO mix.[24]

Insights into the interactions of LCNPs with bilayer membranes have also been gained from cell interaction studies. MO-LCNPs stabilised by either Pluronic F127 or F108 copolymers were observed to alter the lipid distribution and membrane structures of HeLa cells (human cervical carcinoma cells), resulting in lipid droplet accumulation, mitochondrial hyperpolarization and mitochondrial reactive oxygen species (ROS) generation.[25, 26, 27]

Furthermore, Dyett *et al.* observed individual MO-LCNPs interact with the cell membranes of small intestine epithelial cells and STO fibroblasts (Sandos inbred mice (SIM) 6-thioguanine-resistant, ouabain-resistant cell line) by docking onto the membrane surface before diffusing into the membrane, suggestive that the MO incorporates into the cell membrane structure,[21] analogous to reported interactions with minimal model membrane systems.[22, 24]

Current studies have shown strong evidence for the interaction and mixing of LCNPs with bilayer membranes with synergies between findings in model membranes and live cells. However studies in cell-sized unsupported model membranes are missing that would provide greater fundamental insight into the dynamic processes that might occur in unsupported membranes seeded with topologically-active MO-LCNPs. Here we bridge this gap by applying time-resolved confocal fluorescence microscopy to study the interaction between MO-LCNPs and DOPC-GUVs and the dynamic processes during re-equilibration. We reveal a rich diversity and interplay of membrane topological and shape changes that mimic many of the processes of living cellular membranes. These findings shed new light on the potential cellular interaction mechanisms of LCNPs in drug delivery systems as well as underpin the potential of LCNPs as topologically active triggers for membrane remodelling events in artificial cell technologies.

Results

Incorporation of MO from LCNPs into the lipid bilayer causes GUV growth

LCNPs composed of MO stabilized by Pluronic F127 were assembled by hydration of a dried lipid film and sonication. Small angle X-ray scattering (SAXS) characterisation demonstrated that the LCNPs were in the Im3m inverse bicontinuous cubic phase (**Fig. S1a**). **Figure 1b** shows the ‘primitive’ minimal surface with crystallographic space group Im3m. LCNPs had an average hydrodynamic diameter of 179 ± 19 nm and a polydispersity index (PDI) of 0.172 ± 0.005, determined by dynamic light scattering (DLS) (**Fig. S1b**). Cryogenic Transmission Electron Microscopy (cryo-TEM) revealed the structure of the dispersed LCNPs,

with a fast Fourier transform (FFT) image analysis, confirming the internal Im3m crystal structure (**Fig. S1c**).

An initial LCNP concentration screen between 0.95 and 6.7 mg/ml MO mixed with DOPC GUVs using confocal fluorescence microscopy revealed a range of behaviours from rich morphological transformation in the GUVs at low concentration, seen after approximately 2 to 5 minutes, to significant destabilisation and destruction of GUVs at high concentration. From this initial screen, a LCNP concentration of 1.4 mg/ml MO and a MO/DOPC molar ratio of ~250 was selected for further investigation as, under these conditions, rich structural changes were observed in the GUVs over the experimental time window of approximately 20-30 min. We note that the general vesicular architectures of GUVs were stable within the studied time frame.

LCNPs were found to incorporate within the membranes of GUVs. LCNPs labelled with 0.5 mol% NBD-PE were mixed with Rhod-PE labelled DOPC GUVs (1.4 mg/ml MO and MO/DOPC ≈ 250 mol/mol). A uniform signal from the LCNPs was observed at the GUVs membrane surface, indicating that the lipid components of the LCNPs had incorporated within the bilayer structure of the GUVs as simple adsorption of LCNPs on the GUV surface would be observed as punctate spots of fluorescence at the GUV membrane (**Fig. 1c**). This is in agreement with previous studies, showing that LCNPs can adsorb into the DOPC membrane surface.[23, 28, 29, 30] The kinetics of LCNP incorporation into GUV membranes was measured (**Fig. 1d, e)**. Over 13 min, the Rhod-PE probe intensity in the GUV membranes decreased as it was diluted by MO lipids that fused into the membrane structure (**Fig. 1e**). A proportional increase in NBD fluorescence intensity at the GUV membrane correlates with this Rhod-PE intensity decrease. The GUV membrane surface area is also seen to increase in a correlated GUV growth process. For example, in **Figure 1b**, the GUV diameter increased by a factor of 1.4 in 14 min, which corresponds to the surface area increasing by a factor of ~ 2. Consistent with this observed GUV growth, the dilution of Rhod-PE in the membrane showed a decrease in fluorescence intensity by a factor of ~2.2.

GUV growth in response to LCNP addition was also observed to correlate with an increase in membrane permeability. A membrane-impermeable dextran (10 kDa) labelled with Alexa Fluor 488 (AF488) or Cascade Blue was added to the extra-vesicular medium. These passive membrane permeability probes were observed to leak into the lumen of the GUVs over time. GUV leakage to these probes was observed to be stochastic and hence variable between different GUVs in a sample, evident by the different degrees of dextran leakage shown in **Fig. 1f** with unleaked, partially leaked and fully leaked GUVs. Further evidence for the stochastic enhanced permeability of the GUVs induced by MO lipids can be seen in the correlation between vesicle growth (or swelling) and the onset of vesicle leakage (**Fig, S2**).

Generally, GUV permeabilisation occurs near-simultaneously or with a lag time compared to GUV growth from the fusion of MO lipids into the bilayer structure. We attribute the influx of large macromolecules such as 10 kDa dextran into the lumen of the GUVs to be induced by the formations of pores in the vesicle membrane.[31, 32] This is likely due to the enhanced curvature elastic stress in the GUV membranes due to the non-bilayer preferring MO lipids, which favour highly curved structures such as toroidal pores. The stochastic resistance to leakage by some GUVs in the sample is suggestive that the enhancement of membrane permeability might be suppressed under appropriate conditions, such as different GUV membrane compositions.[20, 21] After the GUVs were observed to swell during a growth process induced by MO incorporation, a stability limit appeared to be reached, beyond which a rich array of morphological transitions was observed in the GUVs.

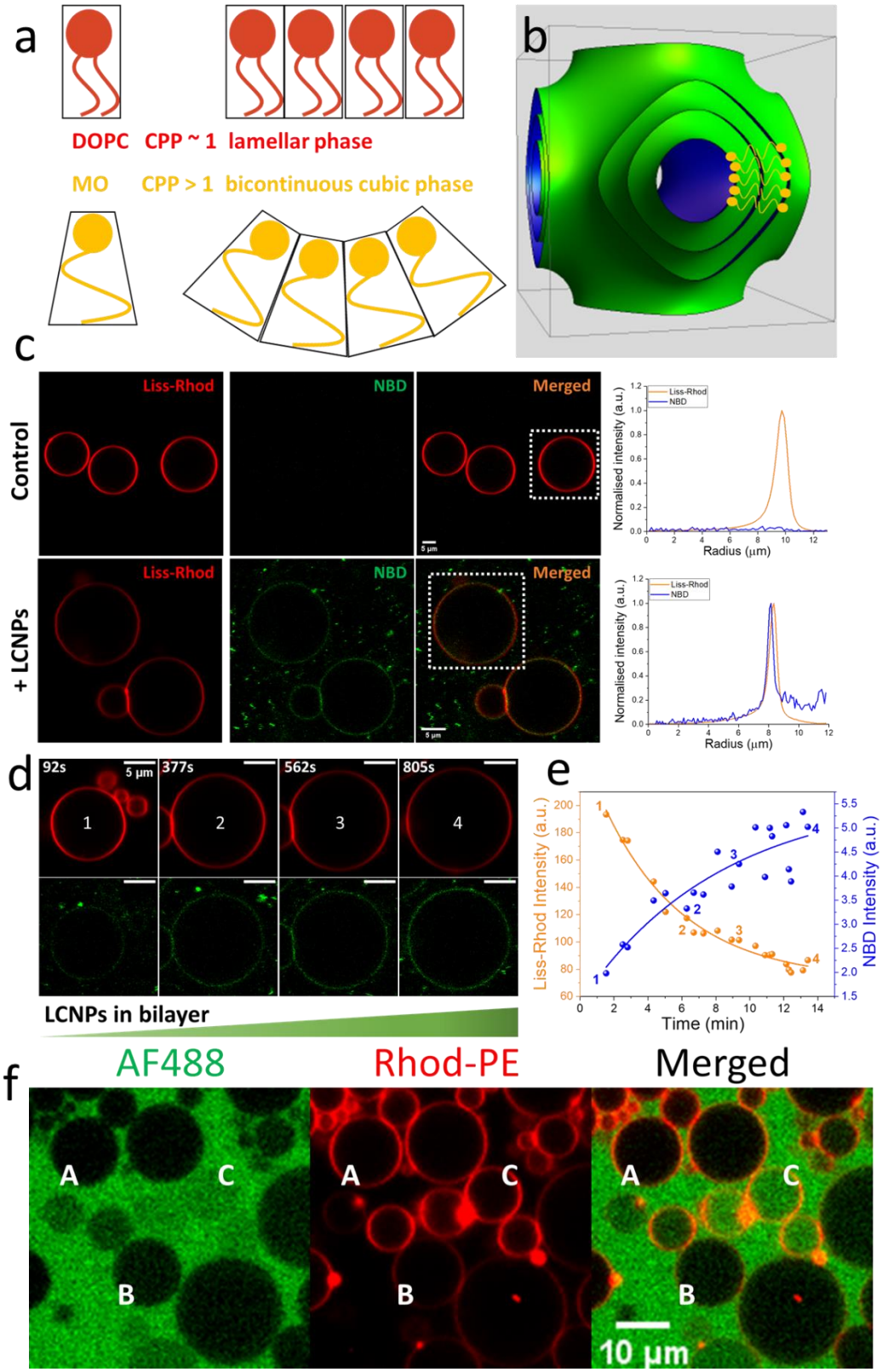

Figure 1: GUVs swell and become permeable after the addition of MO LCNPs (1.4 mg/ml MO; MO/DOPC ≈ 250 mol/mol). (a) Schematic depicting the molecular shapes of DOPC and MO, their critical packing parameters (CPP) and preferred self-assembly polymorphs; (b) The minimal surface of the primitive Im3m bicontinuous cubic phase; (c) The incorporation and homogenous distribution of NBD-PE labelled LCNPs (green) on the surface of GUVs labelled with Rhod-PE (red). Intensity profiles

before and after addition of NBD-PE labelled LCNPs are shown on the right; (d) Real-time observation of LCNPs incorporation into Rhod-PE labelled GUV membranes.; (e) NBD-PE LCNP probe intensity increases while Rhod-PE GUV intensity decreases with time. (f) GUVs labelled with Rhod-PE with different degrees of permeability to 10 kDa dextran labelled with AF488: unleaked (< 25% fluorescence leakage) GUV (A), partially leaked (25 ~ 80 % fluorescence leakage) GUV (B), and fully leaked (> 80% fluorescence leakage) GUV (C).

MO LCNPs bring DOPC GUVs to life by triggering a cascade of dynamic shape and topological transformations.

Incorporation of MO-LCNPs into DOPC-GUVs is expected to create a significant stored curvature elastic stress in the membrane. Non-bilayer-forming MO lipids (spontaneous curvature = −0.054 ± 0.003 $Å^{-1}$) have an inverted cone shape that prefers curved membranous interfaces,[33] such as in the Im3m cubic phase. This contrasts with the near-cylindrical shape of DOPC lipids (spontaneous curvature = −0.0091 ± 0.0008 $Å^{-1}$) that preferentially aggregate as bilayer membranes.[34] Increasing concentration of MO lipids in the GUV membrane enhances the lateral pressure profile in the hydrophobic core of the bilayer such that each lipid monolayer wants to bend towards the hydrating aqueous medium. Once the MO concentration reaches a critical threshold, these stored stresses are observed to release through a range of GUV morphological transitions.

Nanotubes

Within a few minutes following the addition of LCNPs to DOPC GUVs, the majority of vesicles developed lipid tubes protruding from the membrane. These tubes varied in size and direction (into the extra-vesicular medium or the interior lumen). Thin cylinder-like (**Fig. 2a**) and thick unduloid-like (**Fig. 2b**) external nanotubes were observed to protrude from the parent GUV toward the extra-vesicular medium. We also observed internal lipid nanotubes originating at the surfaces of the GUV and protruding into the vesicle lumen (**Fig. 2c**). Both external and internal tubes are undulating and wavy, while some of them form an undulatory pearling pattern. Dynamic fluctuations in all morphologies of both external and internal tubes were observed, suggesting that the incorporation of MO into the DOPC membrane facilitates the

membrane to be highly flexible. In addition, the fluorescence of water-soluble membrane permeability probes in the internal nanotubes indicates that they have an open neck that connects to the extra-vesicular medium (**Fig. 2c**).

Previous studies have reported the pearling instability of GUV nanotubes when the membrane is subject to tension caused by bilayer asymmetry.[35] In our experiments, it is unclear whether LCNP fusion into the GUVs creates bilayer asymmetry or not. Asymmetry exists in terms of the LCNP interaction with the GUV membrane, which is exclusively from the extra-vesicular side of the membrane. However, the rate of MO flip-flop across the bilayer is unknown and any potential asymmetry cannot be resolved from our fluorescence microscopy methods. Lipid flip-flop may occur through collective formation of transmembrane pores, which we often observe after a lag time following GUV growth. Pearling instabilities were mostly observed in unleaked GUVs. Therefore, we speculate that asymmetric membrane stresses from enhanced MO localisation in the outer membrane monolayer of GUVs drives the pearling of lipid tubules that are observed.

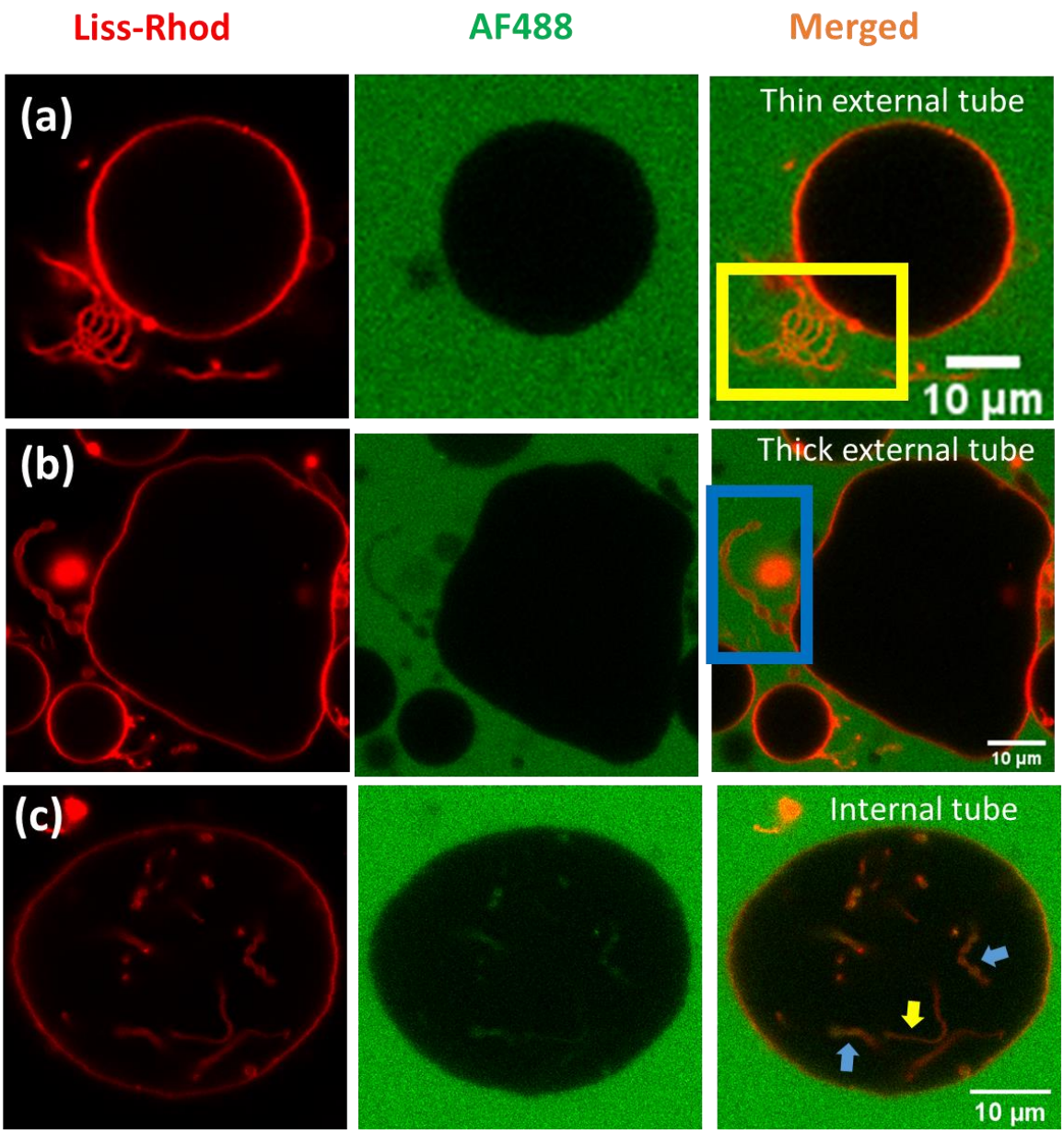

Figure 2. Membrane tubulation following initial growth of GUVs after being fed with MO LCNPs. Thin (a) and thick (b) external lipid nanotubes protrude from vesicles toward the extravesicular medium; (c) thin (yellow arrows) and thick (blue arrows) internal lipid nanotubes that have originated at the surfaces of the GUVs and protrude into the vesicle lumen. Membrane-impermeable dextran (10 kDa) labelled with Alexa Fluor 488 (green) was observed in the internal nanotubes.

Fusion and fission

GUV fission and fusion events were also observed following the addition of LCNPs. To study these phenomena in more detail, two populations of DOPC GUVs labelled with different fluorescent probes were mixed prior to the addition of LCNPs. The two distinctly labelled

populations of GUVs can therefore report on lipid mixing phenomena between adjacent vesicles. One GUV population was labelled with 3,3'-Dioctadecyloxacarbocyanine Perchlorate (DiO; green) and the other GUV population was labelled with Rhod-PE (red, as above).

A typical GUV fusion event is shown in **Fig. 3a**. The contact area between two neighbouring GUVs increases without any observable lipid mixing between the two GUVs. A full fusion pore then opens and the interior lumens of the GUVs mix. This is followed by reconfiguration of the combined GUVs into a single spherical vesicle, where the red and green lipid probes become evenly mixed throughout the membrane by lateral diffusion. Lipid nanotubes that can be seen in the two initial vesicles are conserved within the lumen of the initial fused GUV. However, these tubes disappeared within 2 min of the fusion event, likely retracting into the GUV membrane as the lipid mixture re-equilibrates.

Other fusion-related mechanisms were observed. An example is shown in **Fig. 3b** (**Movie S1**), where a GUV “gives birth” to a smaller GUV from its interior lumen. The interior GUV adheres to the membrane of the outer GUV before translocating to the exterior of this vesicle within a few seconds. We speculate that the internal GUV becomes hemifused with the outer membrane to facilitate this translocation event. It should also be noted that the outer GUV is initially non-spherical and gradually loses its large excess membrane area to become near-spherical during the time course of our observation window (~2 min).

Fusion can also occur between external lipid nanotubes that initially formed on the GUV surface. These tubes have been observed to fuse with one another on a time scale in the order of 10 min, resulting in the formation of many smaller, spherical GUVs (**Fig. 3c)**.

Analogous to membrane fusion, membrane fission was also observed. The excess membrane area induced by fusion of LCNPs into the GUV membrane can lead to membrane buds that fission and divide into daughter GUVs (**Fig. 4, Movie S2**). The large excess area and dynamic shape transformations in these vesicles can also lead to vesicles fissioning into multiple daughter GUVs as they re-equilibrate to a spherical GUV geometry (**Fig. 4b**).

Following fusion of LCNPs into GUV membranes, relaxation of fluctuating GUVs with a larger excess membrane area to re-equilibrate back to a near-spherical GUV structure is commonly observed. We characterise the time course of one such GUV in **Fig. 5** (**Movie S1**) in terms of the apparent membrane area and vesicle aspect ratio ($AR = \frac{major\ axis}{minor\ axis}$) over time. The GUV gradually reduces its membrane area and aspect ratio on the time scale of order 80 s until the aspect ratio returns to approximately 1.0 (spherical shape).

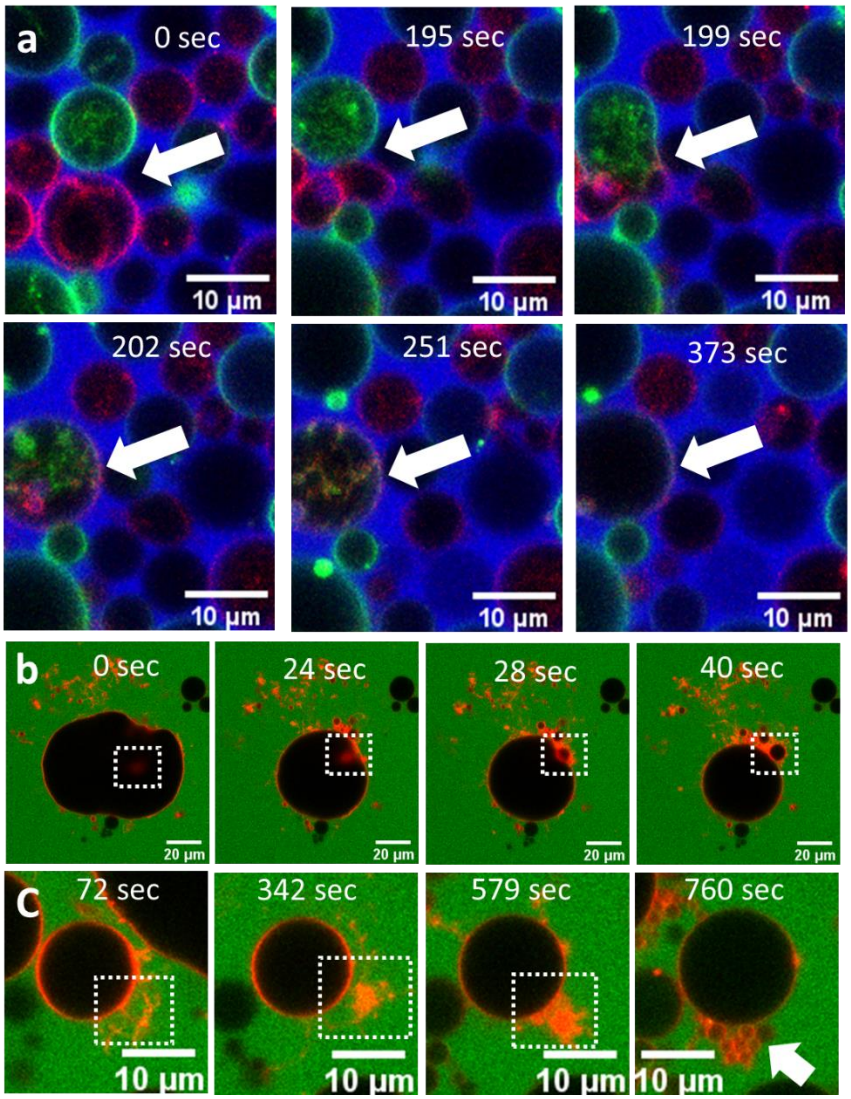

Figure 3. LCNPs trigger fusion events between GUVs or lipid nanotubes. (a) Full fusion of two individual vesicles labelled with DiO (green) and Rhod-PE (red) respectively; (b) An internal vesicle fuses with the outer GUV before translocating to the vesicle exterior. (c) The formation of several small spherical vesicles from the fusion of external lipid nanotubes.

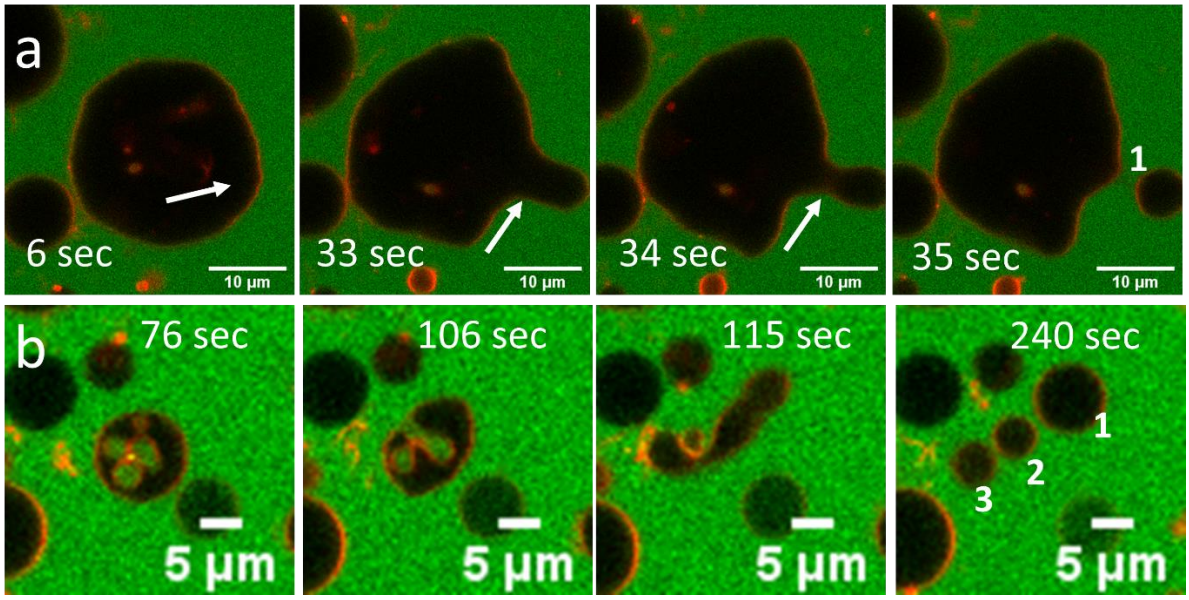

Figure 4. Vesicle fission induced by LCNPs. The white arrows indicate the positions of where the membrane neck closes. The labelled numbers show new vesicles generated by fission events. (a) The "mother" vesicle generates one smaller GUV; (b) the "mother" vesicle separates into three smaller GUVs.

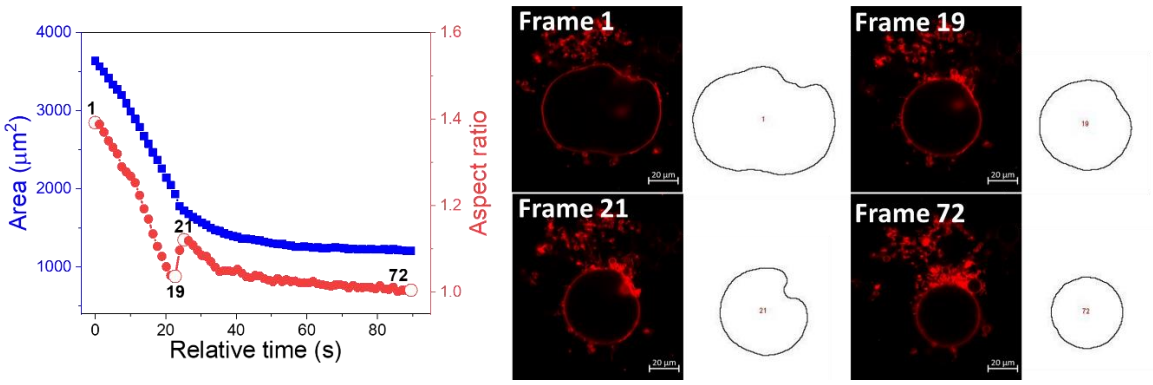

Figure 5. Kinetics of GUV re-equilibration to a spherical shape. Graph of GUV surface area and aspect ratio vs time (left). Representative GUV images from Movie S1 and the extracted GUV outline (right).

Intraluminal vesicles (ILVs)

Membrane topological changes through fusion and fission processes can lead to the generation of new internal lipid compartments inside GUVs: intraluminal vesicles (ILVs). To investigate ILV formation, where extra-vesicular media is encapsulated within these new compartments, a membrane-impermeable 10 kDa dextran labelled with Alexa Fluor 488

(AF488) or Cascade Blue (CBlue) was added to the bulk medium. Formation of ILVs is characterised by the inclusion of AF488 or CBlue in the lumen of these internal vesicles.

We observed three different pathways for ILV formation, summarised in **Fig. 6**. In **Fig. 6a** (**Movie S3**), internal lipid nanotubes that include the external CBlue probe remodel into discrete ILVs that also encapsulate CBlue from the bulk medium. A second mechanism saw two separate GUVs undergo a fusion mechanism, where two independent fusion pores form in the adhesion contact area, such that the membrane in the adhesion plaque becomes scissioned inside the new GUV and encapsulates the AF488 probe (**Fig. 6b, Movie S4**). A final ILV formation mechanism was observed when a non-spherical GUV with larger excess membrane area undergoes membrane fluctuations that lead to a discocyte GUV shape folding around such that the spheroidal end-caps of this structure contact and fuse. This topological transition leaves a CBlue-encapsulating ILV trapped inside an outer membrane (**Fig. 6c, Movie S5**).

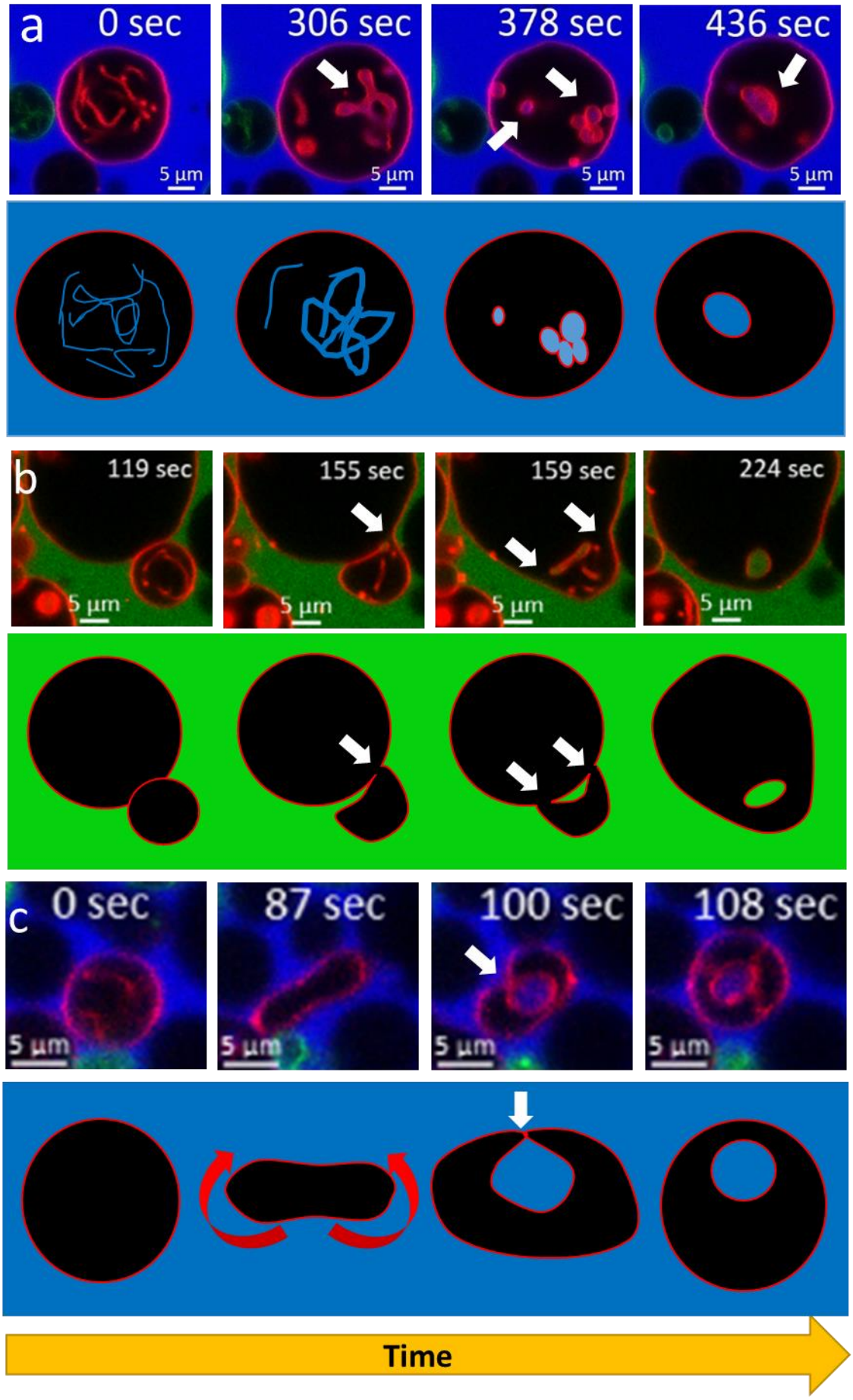
a
0 sec
306 sec
378 sec
436 sec
5 µm
b
119 sec
155 sec
159 sec
224 sec
c
0 sec
87 sec
100 sec
108 sec
Time

284

Figure 6. Intraluminal vesicles can form by different mechanisms. (a) Internal nanotubes fuse to form ILVs. White arrows indicate thin tubes that first fuse to form thicker tubes before forming small ILVs, which continue to fuse into a larger ILV. (b) Two individual vesicles fuse in a mechanism that leads to a trapped ILV. White arrows indicate fusion at each edge of the membrane contact area during fusion. (c) Wrapping of a discocyte GUV leads to fusion of the end caps and formation of an ILV. Red arrows represent the movement of the vesicle and white arrows show fusion of the membrane. In all cases, ILVs are filled with external medium that contains the membrane-impermeable AF488 or CBlue dextran (10 kDa).

Buds

The final re-equilibrated state of the GUVs often resulted in remaining excess membrane area being taken up in membrane buds at the GUV surface. These small buds often have a high fluorescence intensity, suggesting that they may be multilamellar structures (**Fig. 7**). The estimated composition of the MO and DOPC mixture in these buds would favour lamellar structures, based on previous small angle X-ray and neutron reflectivity experiments [24, 36] (note, the MO to DOPC ratio was about 45 mol%; see also discussion below). Neutron scattering studies have revealed an initial rapid adsorption of intact LCNPs at the DOPC bilayer interface, followed by exchange of lipids. Furthermore, SAXS confirmed the strong interaction between LCNPs and DOPC vesicles including unilamellar and multilamellar that initially leads to changes in the size of the unit cell of the cubic phase before transition to the lamellar structure (DOPC/MO molar ratio of 0.01-0.18).

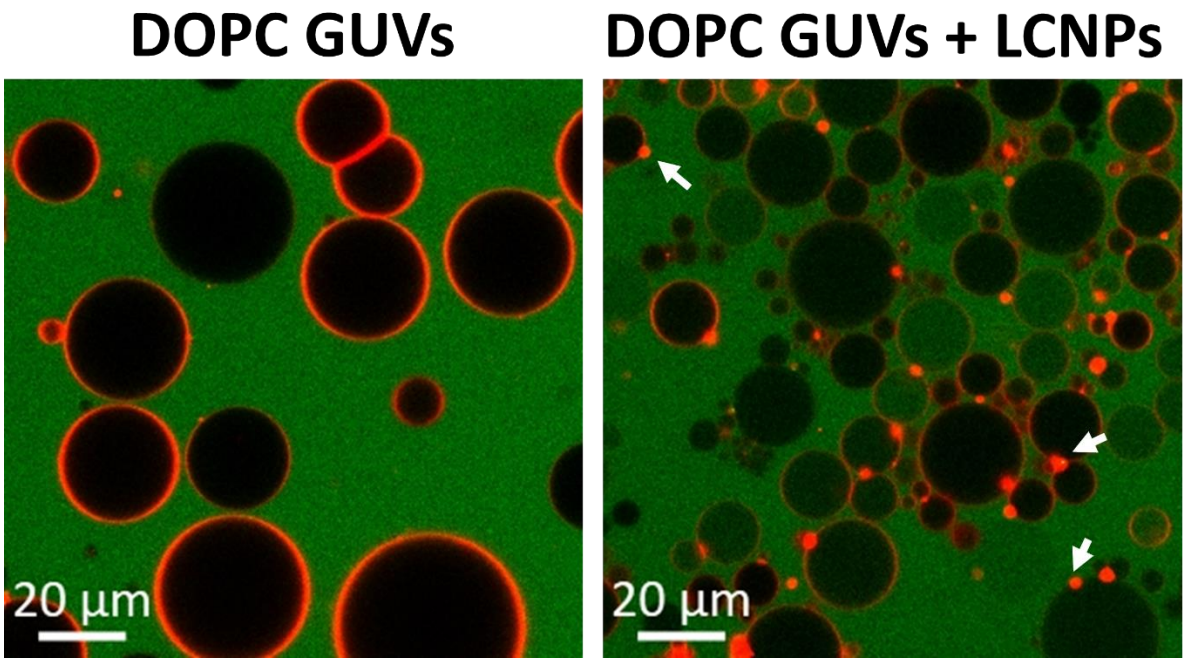

Figure 7. DOPC GUVs before (left) and after (right) LCNPs addition. Following equilibration after LCNP addition, red buds with high fluorescence intensity were observed at the edge of GUVs (white arrows indicate some example buds within the image).

Discussion

We have observed a rich variety of morphological and topological transitions in DOPC GUVs induced by MO-LCNPs in the Im3m cubic phase. These LCNPs fuse into the GUV membrane, increasing the excess membrane area and seeding the membrane with enhanced topological Gaussian curvature energy that lowers the energy barrier to the observed fission, fusion and tubulation processes. The interplay between these different morphological changes is summarised in **Fig. 8.**

The observations presented here are at a MO concentration of 1.4 mg/ml, which results in a MO/DOPC molar ratio of ~250. However, this is not the molar ratio of MO/DOPC in the mixed GUV membranes. The average swelling ratio of GUVs with an average diameter of 11 ± 4 µm was found to be 19 ± 11% within 20 min of LCNP incubation (**Table S1**). Taking the molecular surface area of DOPC to be 0.72 nm^2,[37] and the polar molecular surface area of MO to be 0.33 nm^2,[38] we estimate the average molar ratio of MO in the GUV membrane to be

45 ± 17 mol%. Comparing our calculation to the phase diagram of MO/DOPC,[39] where equilibrium mixtures are found to be in the lamellar L_α phase up to ~75 mol% MO, we predict that these mixed systems are still in the lamellar phase of the equilibrium phase diagram within the studied time scale. At this ~45 mol% MO composition, the membranes dynamically undergo morphological transitions that re-equilibrate the GUVs by decreasing the excess membrane area until they return to their near-spherical final state. Note that fission and fusion events during the studied time scale will decrease or increase the swelling ratio, which might affect the calculated number of LCNPs incorporated per GUV.

At higher concentrations of MO-LCNPs, GUVs can become rapidly destabilised and destroyed. Here, the kinetics of MO incorporation into the GUV membrane will increase. We propose that under these conditions the increasing MO concentration in the membrane may pass the lamellar-cubic phase boundary (~75 mol% MO in the MO/DOPC membrane), where the faster kinetics of the lamellar to cubic phase transition occur before the slower dynamics of membrane topological and morphological transitions can occur.

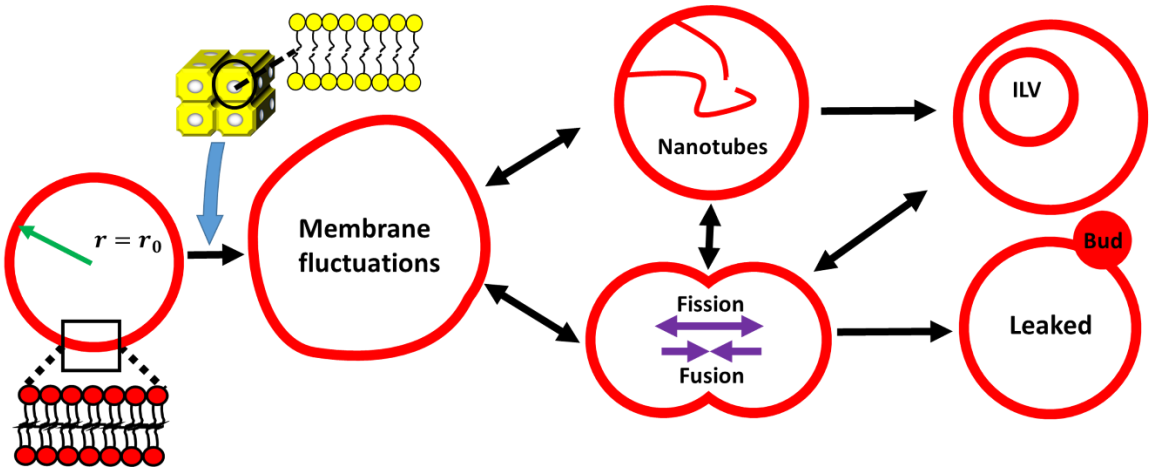

Figure 8. Schematic representation of morphological changes of DOPC GUVs induced by MO-LCNPs (cubosomes).

These fundamental new findings on the interaction of cubic phase LCNPs with lamellar GUV membranes will provide vital insights into a number of scientific questions and applications. Firstly, this approach might be able to provide new fundamental insight into the role of the Gaussian curvature modulus in vesicle fission and fusion.[40] By seeding lamellar GUVs with cubic phase forming lipids, the Gaussian curvature modulus of the GUV membrane might be controllably and systematically tuned. The major technical challenge with this approach is that the mechanical moduli of mixed membrane systems are not linearly additive based upon the moduli of each single lipid component in the mixture. However, a semi-quantitative approach may be the best strategy forward here.

Our approach holds promise for the bio-engineering field of artificial cells.[41, 42] Dynamic topological changes such as fusion and fission are essential functional processes in living cells and hence are highly desirable features to engineer into minimal artificial cells.[43, 44, 45, 46] To enhance this approach for the engineering biology toolbox, the leakage of GUV contents should be minimised to prevent loss of vital functional biomolecules from the GUV lumen, and further regulation of the interactions between LCNPs and GUVs might direct the morphological and topological transitions towards a specific mechanism (e.g., fusion, fission, ILV formation). Our findings here present important first steps in gaining control over membrane remodelling processes that will lead to simplified and enhanced mechanisms for regulating dynamic processes in artificial cell membranes.

Cubosome nanoparticles are of interest for nanomedicine drug delivery systems.[9, 47, 48] Their high internal surface area gives a high potential drug loading capacity, but the higher curved nature of cubic phase lipid assemblies is also thought to be relevant in inducing topological changes in the cell that facilitate cell entry and endosomal escape.[21, 47, 49, 50] Fundamental studies of LCNP-GUV interactions may assist with understanding different mechanisms of nanoparticle delivery in cells and also unwanted side effects of cell toxicity that needs to be minimised to facilitate translation to clinical applications

Conclusion

Here we have presented new insights into the interactions of cubosome nanoparticles with bilayer lipid membranes, important to our understanding of cubosomes as drug delivery systems and their application in other bioengineering technologies, such as synthetic biology. Our observations reveal a rich array of morphological and topological transitions driven by the kinetics of adsorption of MO-LCNPs into the lipid bilayer and equilibration processes within the GUV once seeded with excess area and enhanced stored curvature stress in the membrane. The new insights and understanding we have presented in this study are not achievable in previous work on planar bilayer membranes, where the membrane dynamics are suppressed by a solid support, or in living cells, where deep mechanistic insight is frustrated by the complexity of living matter. Future exploration of the broad parameter space of the structure and composition of LCNPs and GUV membranes will promote optimisation of drug delivery and artificial cell technologies.

Methods

Monoolein (MO) cubosomes were prepared by resuspending MO thin films (5 wt%) into an aqueous buffer (10 mM phosphate buffer, 2.7 mM potassium chloride and 137 mM sodium chloride, pH 7.4) in the presence of Pluronic F127 (6.92 mg/ml) as a stabiliser followed by pulse sonication. MO cubosomes were characterised by small angle x-ray scattering (SAXS), dynamic light scattering (DLS) and cryogenic transmission electron microscopy (cryo-TEM). DOPC GUVs containing 0.5 – 1 mol% fluorescent lipid (Rhod-PE or DiO) were formed by electroformation in a 300 mM sucrose solution on ITO glass plates. Confocal microscopy was performed using a Zeiss LSM 880 + Airyscan confocal microscope. Image analysis was conducted using the ZEN Blue version 3.2 (Carl Zeiss Microscopy, Jena, Germany) and Fiji software (National Institute of Mental Health, Maryland, USA).[51] Full materials and methods are described in the supplementary information.

Acknowledgements

We thank Dr Sally Boxall and Dr Ruth Hughes from the Bio-imaging and Flow Cytometry Facility at University of Leeds for their support on the confocal microscopes. We thank Dr Rebecca Thompson and Dr Daniel Maskell from the Astbury Biostructure Facility at University of Leeds for the assistance with Cryo-TEM. We thank Dr Rashmi Seneviratne, Dr Marcos Arribas Perez and Dr Andrew Booth from School of Chemistry at University of Leeds for assistance on GUV preparation and fluorescence image analysis. We also thank Diamond Light Source for the award beamtimes (SM26258-1, SM19127) as well as Dr Sam Burholt, Dr Tim Snow, Dr Andy Smith and Professor Nick Terrill for their support and assistance. We further acknowledge the EPSRC as the funder of the DL-SAXS facility (grant no. EP/R042683/1).The LSM880 + Airyscan confocal microscopes used were funded by the Wellcome Trust (WT104918/Z/14/Z). The FEI Titan Krios microscope used was funded by the University of Leeds (UoL ABSL award) and Wellcome Trust (108466/Z/15/Z). The research was supported by start-up funding awarded to A.I.I.T. from the University of Leeds as a well

as a PhD scholarship awarded to Z.X. PB acknowledges funding from the Engineering and Physical Sciences Research Council (EPSRC; grant nos. EP/M027929/1 and EP/R03608X/1). The Bragg Centre for Materials Research at the University of Leeds is also acknowledged.

Author contributions

Z.X., A.I.I.T. and P.A.B. conceived and designed the research. Z.X. performed the experiments and analysed the results. Z.X., M.R., A.I.I.T. and P.A.B. wrote the paper and interpreted the results.

Competing interests

The authors declare no competing interests.

Correspondence and requests for materials should be address to A.I.I.T. and P.A.B.

References

1. van Meer G, Voelker DR, Feigenson GW. Membrane lipids: where they are and how they behave. *Nature Reviews Molecular Cell Biology* **9**, 112-124 (2008).

2. Klose C, Surma MA, Simons K. Organellar lipidomics—background and perspectives. *Current Opinion in Cell Biology* **25**, 406-413 (2013).

3. Almsherqi ZA, Kohlwein SD, Deng Y. Cubic membranes: a legend beyond the Flatland* of cell membrane organization. *Journal of Cell Biology* **173**, 839-844 (2006).

4. Zhai J, Fong C, Tran N, Drummond CJ. Non-Lamellar Lyotropic Liquid Crystalline Lipid Nanoparticles for the Next Generation of Nanomedicine. *ACS Nano* **13**, 6178-6206 (2019).

5. Tenchov R, Bird R, Curtze AE, Zhou Q. Lipid Nanoparticles—From Liposomes to mRNA Vaccine Delivery, a Landscape of Research Diversity and Advancement. *ACS Nano* **15**, 16982-17015 (2021).

6. Guevara ML, Persano F, Persano S. Advances in Lipid Nanoparticles for mRNA-Based Cancer Immunotherapy. *Frontiers in Chemistry* **8**, 963 (2020).

7. van 't Hag L, Gras SL, Conn CE, Drummond CJ. Lyotropic liquid crystal engineering moving beyond binary compositional space – ordered nanostructured amphiphile self-assembly materials by design. *Chemical Society Reviews* **46**, 2705-2731 (2017).

8. Israelachvili JN, Mitchell DJ, Ninham BW. Theory of self-assembly of hydrocarbon amphiphiles into micelles and bilayers. *Journal of the Chemical Society, Faraday Transactions 2: Molecular and Chemical Physics* **72**, 1525-1568 (1976).

9. Barriga HMG, Holme MN, Stevens MM. Cubosomes: The Next Generation of Smart Lipid Nanoparticles? *Angewandte Chemie International Edition* **58**, 2958-2978 (2019).

10. Knorr RL, Mizushima N, Dimova R. Fusion and scission of membranes: Ubiquitous topological transformations in cells. *Traffic* **18**, 758-761 (2017).

11. Carlton JG, Jones H, Eggert US. Membrane and organelle dynamics during cell division. *Nature Reviews Molecular Cell Biology* **21**, 151-166 (2020).

12. McMahon HT, Gallop JL. Membrane curvature and mechanisms of dynamic cell membrane remodelling. *Nature* **438**, 590-596 (2005).

13. Le Roux A-L*, et al.* Dynamic mechanochemical feedback between curved membranes and BAR protein self-organization. *Nature Communications* **12**, 6550 (2021).

14. Hurley JH, Emr SD. THE ESCRT COMPLEXES: Structure and Mechanism of a Membrane-Trafficking Network. *Annual Review of Biophysics and Biomolecular Structure* **35**, 277-298 (2006).

15. Mayor S, Pagano RE. Pathways of clathrin-independent endocytosis. *Nature Reviews Molecular Cell Biology* **8**, 603-612 (2007).

16. Harayama T, Riezman H. Understanding the diversity of membrane lipid composition. *Nature Reviews Molecular Cell Biology* **19**, 281-296 (2018).

17. Lingwood D, Simons K. Lipid Rafts As a Membrane-Organizing Principle. *Science* **327**, 46-50 (2010).

18. Sezgin E, Levental I, Mayor S, Eggeling C. The mystery of membrane organization: composition, regulation and roles of lipid rafts. *Nature Reviews Molecular Cell Biology* **18**, 361-374 (2017).

19. Chang DP, Barauskas J, Dabkowska AP, Wadsäter M, Tiberg F, Nylander T. Non-lamellar lipid liquid crystalline structures at interfaces. *Advances in Colloid and Interface Science* **222**, 135-147 (2015).

20. Dyett BP, Yu H, Sarkar S, Strachan JB, Drummond CJ, Conn CE. Uptake Dynamics of Cubosome Nanocarriers at Bacterial Surfaces and the Routes for Cargo Internalization. *ACS Applied Materials & Interfaces* **13**, 53530-53540 (2021).

21. Dyett BP, Yu H, Strachan J, Drummond CJ, Conn CE. Fusion dynamics of cubosome nanocarriers with model cell membranes. *Nat Commun* **10**, 4492 (2019).

22. Vandoolaeghe P, Rennie AR, Campbell RA, Nylander T. Neutron reflectivity studies of the interaction of cubic-phase nanoparticles with phospholipid bilayers of different coverage. *Langmuir* **25**, 4009-4020 (2009).

23. Vandoolaeghe P*, et al.* Adsorption of cubic liquid crystalline nanoparticles on model membranes. *Soft Matter* **4**, 2267-2277 (2008).

24. Vandoolaeghe P, Barauskas J, Johnsson M, Tiberg F, Nylander T. Interaction between Lamellar (Vesicles) and Nonlamellar Lipid Liquid-Crystalline Nanoparticles as Studied by Time-Resolved Small-Angle X-ray Diffraction. *Langmuir* **25**, 3999-4008 (2009).

25. Falchi AM*, et al.* Effects of monoolein-based cubosome formulations on lipid droplets and mitochondria of HeLa cells. *Toxicology Research* **4**, 1025-1036 (2015).

26. Rosa A, Murgia S, Putzu D, Meli V, Falchi AM. Monoolein-based cubosomes affect lipid profile in HeLa cells. *Chemistry and Physics of Lipids* **191**, 96-105 (2015).

27. Strachan JB, Dyett BP, Nasa Z, Valery C, Conn CE. Toxicity and cellular uptake of lipid nanoparticles of different structure and composition. *J Colloid Interface Sci* **576**, 241-251 (2020).

28. Vandoolaeghe P, Campbell RA, Rennie AR, Nylander T. Adsorption of Intact Cubic Liquid Crystalline Nanoparticles on Hydrophilic Surfaces: Lateral Organization, Interfacial Stability, Layer Structure, and Interaction Mechanism. *The Journal of Physical Chemistry C* **113**, 4483-4494 (2009).

29. Vandoolaeghe P, Tiberg F, Nylander T. Interfacial Behavior of Cubic Liquid Crystalline Nanoparticles at Hydrophilic and Hydrophobic Surfaces. *Langmuir* **22**, 9169-9174 (2006).

30. Chang DP, Jankunec M, Barauskas J, Tiberg F, Nylander T. Adsorption of Lipid Liquid Crystalline Nanoparticles on Cationic, Hydrophilic, and Hydrophobic Surfaces. *ACS Applied Materials & Interfaces* **4**, 2643-2651 (2012).

31. Bergstrom CL, Beales PA, Lv Y, Vanderlick TK, Groves JT. Cytochrome c causes pore formation in cardiolipin-containing membranes. *Proceedings of the National Academy of Sciences* **110**, 6269 (2013).

32. Heuvingh J, Bonneau S. Asymmetric Oxidation of Giant Vesicles Triggers Curvature-Associated Shape Transition and Permeabilization. *Biophysical Journal* **97**, 2904-2912 (2009).

33. Dymond MK*, et al.* Lipid Spontaneous Curvatures Estimated from Temperature-Dependent Changes in Inverse Hexagonal Phase Lattice Parameters: Effects of Metal Cations. *Langmuir* **32**, 10083-10092 (2016).

34. Kollmitzer B, Heftberger P, Rappolt M, Pabst G. Monolayer spontaneous curvature of raft-forming membrane lipids. *Soft Matter* **9**, 10877-10884 (2013).

35. Chaïeb S, Rica S. Spontaneous curvature-induced pearling instability. *Physical Review E* **58**, 7733-7737 (1998).

36. Vandoolaeghe P, Rennie AR, Campbell RA, Nylander T. Neutron Reflectivity Studies of the Interaction of Cubic-Phase Nanoparticles with Phospholipid Bilayers of Different Coverage. *Langmuir* **25**, 4009-4020 (2009).

37. Nagle JF, Tristram-Nagle S. Structure of lipid bilayers. *Biochim Biophys Acta* **1469**, 159-195 (2000).

38. Templer RH. On the Area Neutral Surface of Inverse Bicontinuous Cubic Phases of Lyotropic Liquid-Crystals. *Langmuir* **11**, 334-340 (1995).

39. Cherezov V, Clogston J, Misquitta Y, Abdel-Gawad W, Caffrey M. Membrane protein crystallization in meso: lipid type-tailoring of the cubic phase. *Biophys J* **83**, 3393-3407 (2002).

40. Bassereau P*, et al.* The 2018 biomembrane curvature and remodeling roadmap. *Journal of Physics D: Applied Physics* **51**, 343001 (2018).

41. Schwille P*, et al.* MaxSynBio: Avenues Towards Creating Cells from the Bottom Up. *Angewandte Chemie International Edition* **57**, 13382-13392 (2018).

42. Buddingh' BC, van Hest JCM. Artificial Cells: Synthetic Compartments with Life-like Functionality and Adaptivity. *Accounts of Chemical Research* **50**, 769-777 (2017).

43. Arribas Perez M, Beales PA. Biomimetic Curvature and Tension-Driven Membrane Fusion Induced by Silica Nanoparticles. *Langmuir* **37**, 13917-13931 (2021).

44. Kostina NY*, et al.* Unraveling topology-induced shape transformations in dendrimersomes. *Soft Matter* **17**, 254-267 (2021).

45. Dreher Y, Jahnke K, Bobkova E, Spatz JP, Göpfrich K. Division and Regrowth of Phase-Separated Giant Unilamellar Vesicles**. *Angewandte Chemie International Edition* **60**, 10661-10669 (2021).

46. Lira RB, Robinson T, Dimova R, Riske KA. Highly Efficient Protein-free Membrane Fusion: A Giant Vesicle Study. *Biophysical Journal* **116**, 79-91 (2019).

47. Prange JA*, et al.* Overcoming Endocytosis Deficiency by Cubosome Nanocarriers. *ACS Applied Bio Materials* **2**, 2490-2499 (2019).

48. Azhari H, Younus M, Hook SM, Boyd BJ, Rizwan SB. Cubosomes enhance drug permeability across the blood–brain barrier in zebrafish. *International Journal of Pharmaceutics* **600**, 120411 (2021).

49. Kim H, Leal C. Cuboplexes: Topologically Active siRNA Delivery. *ACS Nano* **9**, 10214-10226 (2015).

50. Deshpande S, Singh N. Influence of Cubosome Surface Architecture on Its Cellular Uptake Mechanism. *Langmuir* **33**, 3509-3516 (2017).

51. Schindelin J*, et al.* Fiji: an open-source platform for biological-image analysis. *Nat Methods* **9**, 676-682 (2012).